

# Charge gaps and quasiparticle bands of the ionic Hubbard model

Torben Jabben<sup>1</sup>, Norbert Grewe<sup>1</sup>, and Frithjof B. Anders<sup>2</sup>

<sup>1</sup> Institut für Festkörperphysik, Technische Universität Darmstadt, D-64289 Darmstadt, Germany

<sup>2</sup> Fachbereich 1, Universität Bremen, D-28334 Bremen, Germany

March 20, 2019

**Abstract.** The ionic Hubbard model on a cubic lattice is investigated using analytical approximations and Wilson's renormalization group for the charge excitation spectrum. Near the Mott insulating regime, where the Hubbard repulsion starts to dominate all energies, the formation of correlated bands is described. The corresponding partial spectral weights and local densities of states show characteristic features, which compare well with a hybridized-band picture appropriate for the regime at small  $U$ , which at half-filling is known as a band insulator. In particular, a narrow charge gap is obtained at half-filling, and the distribution of spectral quasi-particle weight reflects the fundamental hybridization mechanism of the model.

**PACS.** 71.27.+a Strongly correlated electron systems; heavy fermions – 71.10.fd Lattice fermion models (Hubbard model, etc.) – 71.10.+h Metal-insulator transitions and other electronic transitions

## 1 Introduction

Investigations of the ionic Hubbard model have led to an ongoing debate about different types of phases with and without broken symmetries and transitions between them [1, 2]. Reliable information has so far been obtained mainly for the one-dimensional case, where Quantum Monte Carlo methods [3] or the density matrix renormalization group [4] are applicable. From these it became clear, that a site dependent variation of atomic energies can induce critical behaviour and long-ranged correlations which are absent

in the homogeneous Hubbard model. This simple version of the model in one dimension and for the particularly interesting case of half-filling is a correlated Mott insulator for all values  $U > 0$  of the local Coulomb repulsion, with a gap for charge excitations but none for spin excitations. Its critical bond-bond correlations apparently freeze out at low  $T$  in a parameter range  $U_{c1} < U < U_{c2}$ , when the model is chosen ionic. For  $U$  above  $U_{c2}$  spin-spin correlations seem to dominate, so that in a regime, where  $U$  is sufficiently larger than the local energy variation, the

same type of Mott insulating phase is approached as in the nonionic model.

The homogeneous Hubbard model in higher dimensions, namely  $d = 3$ , likewise shows an interesting phase diagram, which e.g. was calculated in the framework of dynamical mean field theory[5]. Apart from regions possibly destabilized by phase separation, magnetic phases prevail for large values of  $U$  near half-filling, whereas upon doping the Mott insulator in form of a correlated paramagnet is increasingly stabilized. In the ionic model this type of state is supposed to be relevant at least for charge excitations and even though additional magnetic order may be involved. It is therefore desirable to investigate a correlated paramagnetic state for the Hubbard model at intermediate  $U$  and small ionicity, where formation of low lying quasi-particle bands can be expected via an interplay of local correlations and inhomogeneous local energies. We will thus concentrate on one-particle excitations in a Fermi liquid phase and study the corresponding spectral functions via appropriate many-body techniques.

In the regime near the metal insulator transition, where  $U$  becomes comparable with the bandwidth as derived from nearest-neighbour transfer, the Hubbard model near half-filling shares an important feature with the Anderson lattice model: Bands of heavy quasiparticles with long lifetimes form at low temperatures. Although in both cases this process is driven by the strong local interactions and involves complicated many-body correlations, some features of the quasi-particle band structure seem to be linked to properties already inherent in the one-body terms of the

Hamiltonian. This applies e.g. to the volume of the Fermi surface due to Luttingers theorem in the Fermi liquid state, but even more detailed structure may be preserved as can be inferred from existing work on these models [6, 7,9,11]. Particularly intriguing is the case of the spectral composition of quasi-particles at different wavenumbers, which one could expect to be largely determined by the structure and symmetry of the fundamental hybridization terms of these models. We will show that indeed this also occurs in the ionic Hubbard model.

Application of the Friedel sum rule and of the Luttinger theorem [12] to the Anderson lattice model allows conclusions about the density of states (DOS) in the region of low lying quasi-particle excitations [13]. In particular for one conduction band and two electrons per site the noninteracting version of the model has a hybridization gap at the Fermi energy, and the Fermi surface coincides with the boundary of the first Brillouin zone, a situation which should be preserved when interactions are included.

More generally, one may argue that a coherent action of the Kondo effect should lead to a gap at the energetic position where the many body resonances form on each lattice site. Then it will depend on the localized charge whether this position is near the Fermi energy and thus leads to a charge excitation gap. Indeed, many-body calculations using various techniques have demonstrated that a picture of hybridized quasi-particle bands is an appropriate description of the low temperature regime of this model [14, 15,16,17,18].

The Hubbard model likewise contains interactions and hybridization terms, the latter usually being addressed as transfers to nearest neighbours. The noninteracting version gives one simple tight binding conduction band, and the generic case puts the Fermi level somewhere near the band center. Correspondingly, the Fermi surface lies well inside the first Brillouin zone and a gap is not expected in the interacting case, too. The situation can change drastically when an ionic Hubbard model is considered. For a bipartite, simple cubic lattice with local one particle energies differing between the two sublattices, the first Brillouin zone is halved, and with one electron per site the Fermi surface coincides with the new, smaller zone boundary. Then it can again be expected that the symmetry-breaking effective field produces enough Bragg scattering to lift the degeneracy at the zone boundary and thus leads to a gap. We would expect therefore on the basis of similarities to the Anderson lattice that at least near half-filling quasiparticle bands form at low  $T$ , which reveal the underlying hybridization mechanism. In addition, it would be interesting to find out, whether the wave vector dependence of the corresponding matrix elements is visible in the results, e.g. in the structure of quasi-particles.

This expectation, in fact, is supported by a theoretical approach, which has proven extremely useful for such models with dominant local interactions. The approach rests upon the picture of effective sites [14], which react to a surrounding medium which in turn is formed by these same local objects. Links between them are established via the same elementary transfer processes which lead to band

formation via tight binding of noninteracting electrons. Scattering of quasi-particles by the effective sites thus reflects in lowest order just the  $\mathbf{k}$ -dependence of these hybridization matrix elements, whereas the important part of the selfenergy remains local, i.e.  $\mathbf{k}$ -independent. Quite a long line of approximations have been formulated along these lines, from the ATA [15] and the Renormalized Band Theory [16] to the XNCA [17] and the Dynamical Mean field Theory (DMFT) [18], which has become very popular. It possesses a sound justification and has formed the basis of extensive studies of Hubbard and Anderson models [9]. Generally, quasi-particle bands of the type outlined above are derived with these methods supporting our view and furnishing a good prospect for generalizations e.g. to the ionic Hubbard model.

Early approaches to the Anderson lattice model like the ATA and the LNCA used simplified versions of the Non-Crossing Approximation (NCA) at finite  $U$  for the calculation of scattering processes by the effective sites. They clearly pointed to a quasi-particle band structure with a hybridization gap. A more consistent description of the effective medium, as contained in the XNCA, put this in doubt for a while, because subtle cancellations between local and nonlocal contributions to the selfenergy do not occur in the right way due to shortcomings of the NCA. When combined with a better local method the selfconsistency cycle of the XNCA produces the gap, too. In combination e.g. with the Numerical Renormalization Group (NRG) [19] this has become a reliable tool, at least for low temperatures and excitation energies. The NCA, as a

well explored and controlled analytical tool, is nevertheless of value in such procedures and can be expected to become even more useful when a full or even an extended version becomes manageable in numerical calculations.

In the following section II we will introduce our model Hamiltonian and discuss shortly the techniques used to solve the model. The transition from the energy levels of isolated ions towards the fully developed picture of correlated quasi-particle bands will be performed in two steps: At first, it is instructive to study the splitted bands furnished by the Free Theory, which neglects all two particle correlations except for the purely local ones and which can be viewed as the generalization of the Hubbard I-approximation. It allows for a discussion of partial densities of states (DOS), interaction - and hybridization - induced band splittings and van Hove singularities in the absence of lifetime effects. Section III contains a version of the theory, which is locally complete (i.e. takes all pseudolocal cumulant vertices into account) and may be regarded as the appropriate version of the DMFT. Calculations are carried out with an analytical impurity solver, a simplified version of the finite  $U$  - NCA [20], and alternatively with the NRG. Whereas the former allows for a qualitative study of lifetime effects and is particularly useful at higher excitation energies, a clear cut picture of hybridization effects in the region of the many-body resonance is only achieved with the latter. The final section IV contains a short discussion and concluding remarks about future perspectives.

## 2 The bipartite Hubbard model and correlated bands

We build our model with two sorts of  $s$ -shells with one particle energies  $\varepsilon_A, \varepsilon_B = \varepsilon_A + \Delta$  and local Colomb matrix elements  $U_A, U_B$ . Each of them is placed onto one sublattice  $L_A, L_B$  of a three-dimensional simple cubic lattice, so that the nearest neighbours of one sort belong to the other. The Hamiltonian is:

$$\begin{aligned}
 H &= H_A + H_B + H_{AB} \quad \text{with} \\
 H_\nu &= \sum_{j \in L_\nu} \left( \sum_\sigma \varepsilon_{\nu j \sigma} + U_\nu n_{\nu j \uparrow} n_{\nu j \downarrow} \right) = \\
 &= H_\varepsilon^{(\nu)} + H_U^{(\nu)} \quad (\nu = A, B), \\
 H_{AB} &= t \sum_{j \in L_A} \sum_{\ell \in L_B \text{ n.N. of } j} a_{j\sigma}^+ b_{\ell\sigma} + h.c. . \quad (1)
 \end{aligned}$$

We have introduced the local occupation operators  $n_{Aj\sigma} = a_{j\sigma}^+ a_{j\sigma}$  and  $n_{B\ell\sigma} = b_{\ell\sigma}^+ b_{\ell\sigma}$  for sites on each sublattice and absorbed the (common) chemical potential into the one particle energies. A scheme of the resulting energies of local shells is shown in Fig. 1, which also gives an impression of the energy regime we have in mind when the indicated position of the Fermi level and the zeroth order bandwidths are recognized.

This atomic limit is described by the Hamiltonian  $H_A + H_B$ . If the transfer term is added instead of the interactions, i.e. when

$$H_{U=0} = H_\varepsilon^{(A)} + H_\varepsilon^{(B)} + H_{AB} \quad (2)$$

is considered, a picture of hybridized tight binding bands for noninteracting electrons emerges, which is easily visualized: Assuming first  $\Delta = 0$ , the single tight binding band of a homogeneous ( $\varepsilon_A = \varepsilon_B$ ) lattice is folded back

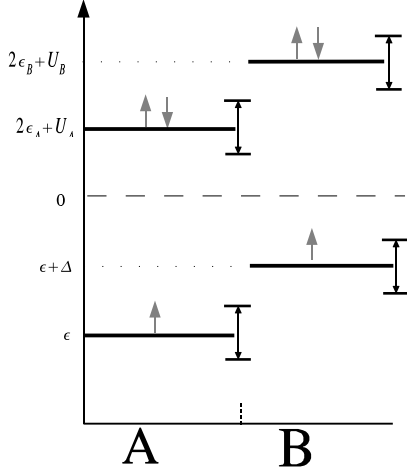


**Fig. 1.** Scheme of the local shells and the energy regime used for the bipartite Hubbard model. The expected bandwidth is indicated by the vertical delimiters. The Fermi level lies well separated between the lower and upper bands.

corresponding to a halving of the Brillouin zone. The effect of  $\Delta$  then shifts the remaining original and backfolded pieces apart, producing gaps due to Bragg-scattering between the boundaries of the new reduced zone. Fig. 2 gives an impression of this band structure, using a single cosine for the dispersion function  $\varepsilon_{\mathbf{k}}^{(0)} = 2t \cos(ka)$  ( $a =$  lattice constant,  $t \leq 0$ ) as appropriate for one dimension.

Shown are the spikes corresponding to the partial DOS

$$\rho_A(\mathbf{k}, \omega) = -\frac{1}{\pi} \text{Im} G_{a_{\mathbf{k}\sigma}, a_{\mathbf{k}\sigma}^+}(\omega + i\delta) \quad (\rho_B \text{ analogous}) \quad (3)$$

derived separately for excitations on each sublattice.

It is easy to see (e.g. perturbatively with respect to  $t$  or with the equation of motion method) that the Greens functions appearing here are given by

$$G_{a_{\mathbf{k}\sigma}, a_{\mathbf{k}\sigma}^+}(z) = \left[ G_A^{(0)}(z)^{-1} - (\varepsilon_{\mathbf{k}})^2 G_B^{(0)}(z) \right]^{-1} \quad (4)$$

$(G_{b_{\mathbf{k}\sigma}, b_{\mathbf{k}\sigma}^+} \text{ analogous}),$

where the counterparts for the noninteracting atomic limit have to be inserted, i.e.

$$G_A^{(0)}(z) = [z - \varepsilon_A]^{-1} \quad (G_B^{(0)} \text{ analogous}). \quad (5)$$

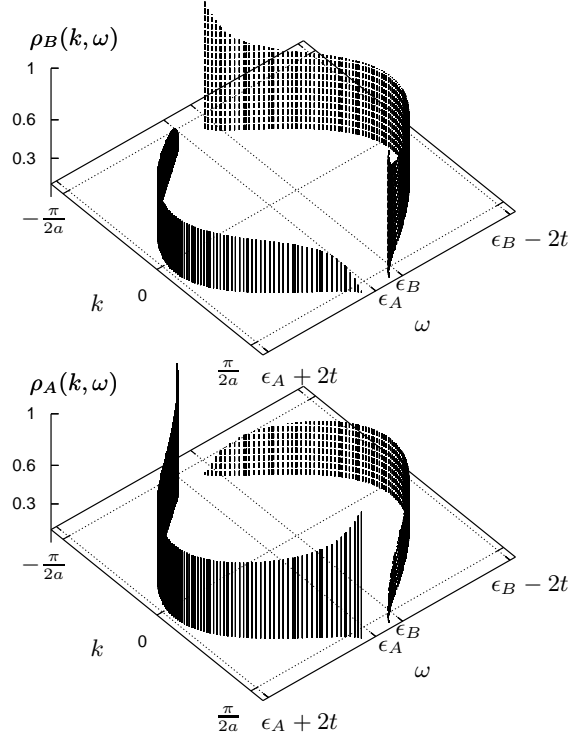


**Fig. 2.** Tight-binding approximation of the one dimensional partial DOS for the A and B sublattice.

Whereas the added spectral weight  $\rho = \rho_A + \rho_B$  would simply exhibit two  $\delta$ -spikes with weight  $\frac{1}{2}$  at the energies of the upper and lower band for each fixed value of crystal momentum  $\mathbf{k}$  and spin  $\sigma$ , the distribution of the partial spectral weights is more interesting, following

$$\rho_A(\mathbf{k}, \omega) = \zeta_A^{(-)}(\mathbf{k}) \cdot \delta(\omega - \varepsilon_{\mathbf{k}}^{(+)}) + \zeta_A^{(+)}(\mathbf{k}) \cdot \delta(\omega - \varepsilon_{\mathbf{k}}^{(-)}),$$

with  $\zeta_A^{(\pm)} = \frac{1}{2} \pm \frac{\Delta}{2\sqrt{\Delta^2 + (2\varepsilon_{\mathbf{k}}^{(0)})^2}},$

$$\varepsilon_{\mathbf{k}}^{(\pm)} = \frac{1}{2} \left( \varepsilon_A + \varepsilon_B \pm \sqrt{\Delta^2 + (2\varepsilon_{\mathbf{k}}^{(0)})^2} \right). \quad (6)$$

For  $\rho_B$  one has to exchange  $\zeta_B^{(+)} = \zeta_A^{(-)}$ ,  $\zeta_B^{(-)} = \zeta_A^{(+)}$ . The gap at the zone boundary equals that of the local states, i.g.  $\varepsilon^{(+)} - \varepsilon^{(-)} = \sqrt{\Delta^2 + (2\varepsilon_{\mathbf{k}}^{(0)})^2} = \Delta$  for  $k = \pm \frac{\pi}{2a}$ , and at these two points the bands terminate in the local energies  $\varepsilon_{\mathbf{k}}^{(+)} = \varepsilon_B$  and  $\varepsilon_{\mathbf{k}}^{(-)} = \varepsilon_A$  for  $k = \pm \frac{\pi}{2a}$ , inducing complete repulsion of admixture from the corresponding other state. Therefore the upper band has full  $B$ -weight at the zone boundaries and less in the middle, whereas the  $A$  weight goes to zero at the boundaries and grows towards the middle of the Brillouin zone and the other way round for the lower band. This simply reflects the shape of the dispersion function  $\varepsilon_{\mathbf{k}}^{(0)}$ , which is zero at the boundaries and has maximal absolute value  $|2t|$  in the zone center, since this function also gives the effective hybridization of electrons with momentum  $\mathbf{k}$  in transfer processes between a site and all of its nearest neighbours.

It is worthwhile to collect these simple facts, since the effects are pertinent and leave their characteristic traces also in the more refined bandstructure derived with better approximations. A popular one in the spirit of Hubbard I, which is called here the Free Theory, can be obtained by simply substituting the Greens functions of the isolated interacting local shells, i.e.

$$G_A^{(1)}(z) = \frac{\zeta_A^{(1)}}{z - \varepsilon_A} + \frac{\zeta_A^{(2)}}{z - \varepsilon_A - U_A} \quad (G_B^{(1)} \text{ analogous}), \quad (7)$$

for the  $G_{A,B}^{(0)}$  given by Eq. (5) in the explicit expressions (4). The resulting bands are derived from a polynomial of fourth order, the zeroes of which are easily determined

numerically, as well as the corresponding partial spectral weights, too. Here we give the explicit dispersion for the special case  $U_A = U_B \equiv U$  and  $T = 0$  where  $\zeta_A^{(1)} = \zeta_A^{(2)} = \zeta_B^{(1)} = \zeta_B^{(2)} = \frac{1}{2}$  in the situation depicted in Fig. 1:

$$\varepsilon_{\mathbf{k}}^{(m)} = \frac{1}{2} \left( \varepsilon_A + \varepsilon_B + U \pm \sqrt{\Delta^2 + U^2 + (2\varepsilon_{\mathbf{k}}^{(0)})^2 \pm 2 \sqrt{(\Delta U)^2 + (U\varepsilon_{\mathbf{k}}^{(0)})^2 + (\varepsilon_{\mathbf{k}}^{(0)})^4}} \right),$$

with

$$\begin{aligned} m \equiv 1 &\hat{=} (+, +), m \equiv 2 \hat{=} (+, -), \\ m \equiv 3 &\hat{=} (-, -), m \equiv 4 \hat{=} (-, +). \end{aligned} \quad (8)$$

The band structure is shown in Fig. 3, where the spectral weights are again resolved in contribution from sublattices  $A$  and  $B$ . Throughout the paper, all energies will be given in units of the hopping parameter  $|t|$ .

One recognizes the same distribution of weight as in the noninteracting case before. The important new feature occurring in the Free Theory is the interaction-induced additional splitting of the hybridized bandstructure, formerly seen in Fig. 2, which is in complete agreement with the phenomenon known from Hubbard's own study: Each of the bands splits in two subbands of approximately half the spectral weight, and differing in energy by roughly the Coulomb repulsion. Interesting is also the corresponding local DOS, which is obtained via summation over all  $\mathbf{k}$ . A glance at the upcoming Fig. 4 shows typical van Hove singularities at the bandedges. In the present bipartite case they may always be attributed to one of the sublattices only, since for the other sublattices the spectral weight vanishes at the corresponding energies. Concluding this section, we comment shortly on the validity of Eq. (4) and

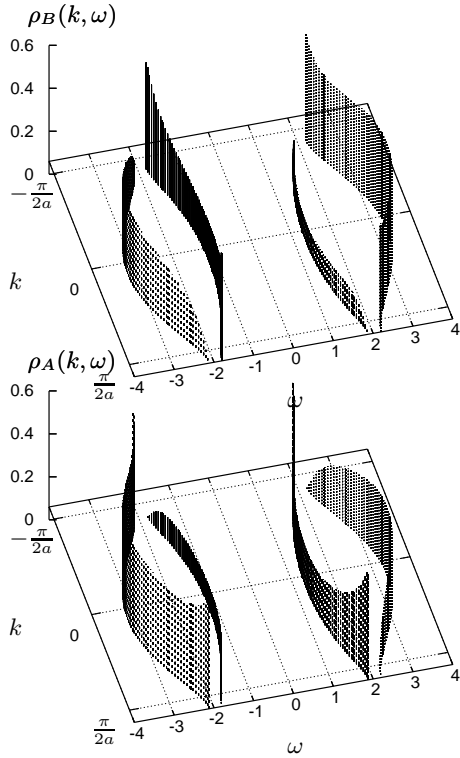


**Fig. 3.** Partial one dimensional DOS of the A and the B sublattice from Free Theory calculations for  $\epsilon_A = -2, \epsilon_B = -1.66, U_A = U_B = 4$ . Due to the energy difference  $\Delta = \epsilon_B - \epsilon_A$  each Hubbard band splits in two subbands with hybridization gaps of width  $\Delta$ .

analogous forms for other inhomogeneous cases as a generalisation of the Hubbard I approximation. The essential point here is the neglect of all nonlocal correlations and thus the restriction to the most important local interaction effect. This is contained in the fractional form of the Greens function (7), which is easily generalized to a more complicated local level structure. Using this Greens function, the approximation simply proceeds as in the noninteracting case, involves the Wick theorem and all benefits

thereof. This may also be disguised as a decoupling in equations of motion.

### 3 Selfconsistent approximations for effective sites and low lying quasi-particle states

Corrections to the Free Theory can be organized perturbatively with help of local cumulant interactions serving as vertices. In order to tackle the infrared problem connected with degeneracies in the metallic regime resummations to infinite order are necessary [21,22]. A well established strategy uses the concept of effective sites, self-consistently coupled to an environment, which is built up by transferring electrons between these same objects. This is accomplished by using an appropriately highly developed technique for an impurity problem and by feeding it with effective propagators for electrons leaving and entering and being scattered in between by other effective sites of the lattice. It is well known how this concept is formally implemented in a small set of equations in an elegant manner [17,18], and we will just state here its generalisation to the present situation with a few comments concerning the role of the quantities appearing.

The two types of lattice sites experience different forms of local one-particle excitation processes, which as before are described via a Greens function in the form

$$G_A(z) \equiv G_{a_{j\sigma}, a_{j\sigma}^+}(z) = \frac{1}{2} \sum_{\mathbf{k}} G_{a_{\mathbf{k}\sigma}, a_{\mathbf{k}\sigma}^+}(z) \quad (G_B \text{ analogous}). \quad (9)$$

For a description of the propagation process inherent in the  $\mathbf{k}$ -dependent Greens function under the sum a divi-

sion into free transfer processes and effective local parts is helpful. This enables one to apply the same reasoning as was used to derive Eq. (4) and thus gives an analogous result here:

$$G_{a_{\mathbf{k}\sigma}, a_{\mathbf{k}\sigma}^+}(z) = [\tilde{G}_A(z)^{-1} - (\varepsilon_{\mathbf{k}})^2 \tilde{G}_B(z)]^{-1} \\ (G_{b_{\mathbf{k}\sigma}, a_{\mathbf{k}\sigma}^+} \text{ analogous}). \quad (10)$$

The effective local Greens functions  $\tilde{G}_A$  and  $\tilde{G}_B$  contain corrections for processes, where particles leave and enter the site along an irreducible loop of transfers. Since such loops on the one hand contribute to the pseudolocal Greens functions  $G_A$  and  $G_B$  and on the other are produced by the free random walk through the lattice leading to the result Eq. (10), these corrections are necessary to avoid overcounting. They are collected in quantities  $\tilde{T}_A(z)$  and  $\tilde{T}_B(z)$ , which enter in the following way:

$$\tilde{G}_A(z)^{-1} = G_A(z)^{-1} + \tilde{T}_A(z) \quad (\tilde{G}_B(z) \text{ analogous}), \quad (11)$$

where  $G_A$  results from Eq. (9). In this way a closed self-consistency cycle is obtained, in the present form with coupled  $A$ - and  $B$ -sublattices, which has to be supplemented as mentioned by an impurity theory for  $G_A$  and  $G_B$ . In the framework of the DMFT [18,8,9], the quantities  $\tilde{T}_{A/B}(z)$  are usually called the dynamical Weiss fields of the theory. Recently it was pointed out [10] that they determine how much the effective local inverse Greens function  $\tilde{G}_{A/B}(z)^{-1}$  has to be deformed to reproduce the  $\mathbf{k}$ -summed lattice Greens function  $G_{A/B}$ .

Analytical impurity solvers have been derived from the noncrossing approximation (NCA) of the Anderson impu-

rity model [23]. Their virtues and shortcomings are well known [24]. A full version of the NCA for finite Coulomb repulsion has been presented long ago [20], but for a quick orientation or for complicated applications usually a simplified version, the SNCA is employed, which needs much less numerical effort. Also improvements of the full NCA have been presented [25,26], which however consume even more time and effort. The SNCA, and to a lesser degree the full NCA, lose their reliability in the regime of very low temperatures and excitation energies. They describe, however, rather well the overall structure and can be used down to temperatures and excitation energies of the order of the many-body scale, connected with the infrared problem, and somewhat below. In particular the full NCA reproduces this nonperturbative scale with quantitative accuracy [20]. We have employed here the SNCA in order to obtain a first test of the selfconsistency cycle outlined in Eqs. (9) to (11). Thereby,  $G_A$  and  $G_B$  are calculated using the loops  $\tilde{T}_A$  and  $\tilde{T}_B$  as input, afterwards one obtains  $\tilde{G}_A$  and  $\tilde{G}_B$  using (11) with these  $G_A$  and  $\tilde{T}_A$ , likewise for  $\tilde{G}_B$ , and finally a new  $G_A$  and  $G_B$  is produced with (10) inserted into (9). These  $G_A$  and  $G_B$  give rise to new loop-expressions  $\tilde{T}_A$  and  $\tilde{T}_B$ , again via Eq. (11), which in turn allow for a new impurity calculation of  $G_A$  and  $G_B$ .

In Fig. 4 results of this iterative procedure are shown and compared to the corresponding quantity calculated in the Free Theory Fig. 4(c) contains the complete local DOS;

$$\rho_{AB}(\omega) = -\frac{1}{2\pi} \text{Im}[G_A(\omega + i\delta) + G_B(\omega + i\delta)] \equiv \\ \equiv \frac{1}{2}[\rho_A(\omega) + \rho_B(\omega)]. \quad (12)$$

and compares it to the corresponding quantity calculated in the Free Theory.

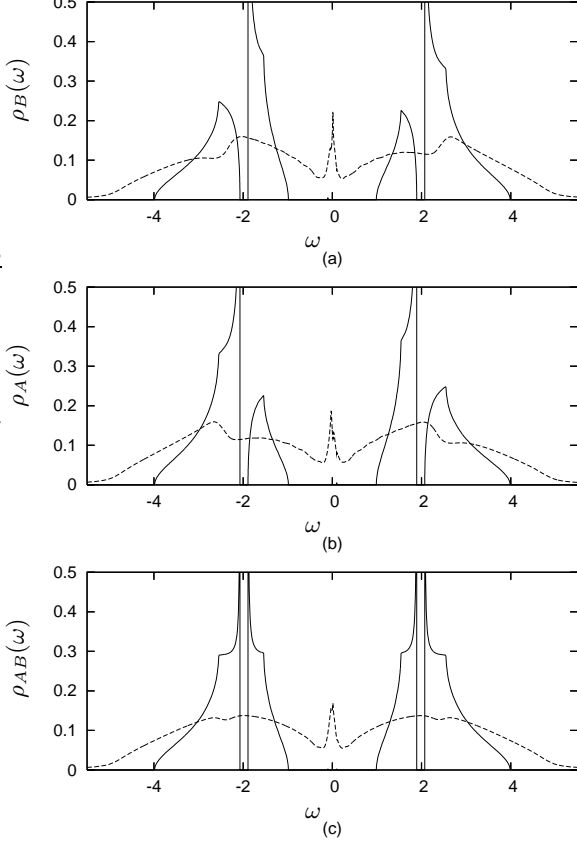


**Fig. 4.** Comparison of the three dimensional local DOS obtained from Free Theory (solid line) and DMFT+SNCA (dashed line) for  $\epsilon_A = -2.07$ ,  $\epsilon_B = -1.89$ ,  $U_A = U_B = 3.96$ ,  $\beta = 20$ .

It is surprising, how much lifetime effects, i.e. the broadening of DOS peaks at fixed  $\mathbf{k}$ , smear out the prominent features of the DOS, which have been discussed in Section 2. The hybridization gaps now only show up as shallow dips and the van Hove singularities have disappeared. The prospect, however, to obtain hybridization-induced gaps in the narrow quasi-particle peak around the Fermi level  $\omega = 0$  are unbroken: The Fermi liquid state guarantees di-

vergent lifetimes for  $T, \omega \rightarrow 0$ . It seems thus encouraging, that the calculation indeed shows some precursor of splitting near  $\omega = 0$ , which is more pronounced in the partial DOS shown in Figs. 4(a) and 4(b). Unfortunately, our selfconsistency cycle with the simplified SNCA tends to become unstable in the most interesting region and does not allow for a more precise investigation of this interesting effect. One should notice from an inspection of Fig. 4, however, that some of the characteristic features of the bipartite lattice, which have been discussed before, survive even in such a locally complete calculation, although only in a smoothed form.

In order to answer reliably the question for hybridization structure in the low energy quasi-particle domain we have finally employed Wilsons renormalization group as the impurity solver in the selfconsistency cycle [27,28,30] defined above. In the meantime, this has become a standard procedure, which essentially improves on the low energy-low temperature results, but due to its logarithmic partition of excitation energies around  $\omega = 0$  tends to suppress important DOS structure elsewhere [29]. This latter statement is substantiated in Fig. 5, viewing the smooth and featureless main resonances near  $\epsilon_A$  and  $\epsilon_A + U_A$ , likewise for  $B$ . At the Fermi level  $\omega = 0$ , on the other hand, this  $T = 0$  calculation reveals a clear and complete hybridization gap in the quasi-particle DOS at the lowest excitation energies. Although the present calculation uses parameter values  $U_A = U_B = 3.96$ ,  $\epsilon_A = -2.07$ ,  $\epsilon_B = -1.89$  near the Mott transition, we expect at least for half-filling this gap to exist at the Fermi level for all values of

$U$  in the Fermi-liquid state, as we have motivated above with reference to the Luttinger theorem.

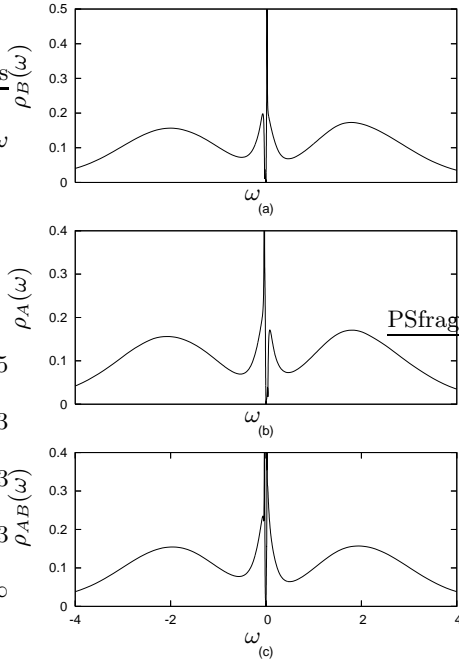


**Fig. 5.** Three dimensional DOS from DMFT+NRG for  $\epsilon_A = -2.07$ ,  $\epsilon_B = -1.89$ ,  $U_A = U_B = 3.96$ ,  $T \rightarrow 0$ . The NRG treatment of the ionic Hubbard model shows a clear quasiparticle hybridization gap at the Fermi level. For the NRG we used  $\Lambda = 2.3$  as discretization parameter [27] and kept  $N_{st} = 700$  states for each NRG iteration.

Moreover, the partial DOS reflects the distribution of spectral weight, which formerly was discussed in connection with the structures at higher energies. Even without  $\mathbf{k}$ -resolution the distribution of spectral weight for the A-lattice near  $\omega = 0$  in Figs. 5(a) and 5(b) resembles the asymmetric shape observed near the hybridization gaps at higher excitation energy in Figs. 4(a) and 4(b), and also the  $\mathbf{k}$ -dependent spectral weight is distributed simi-

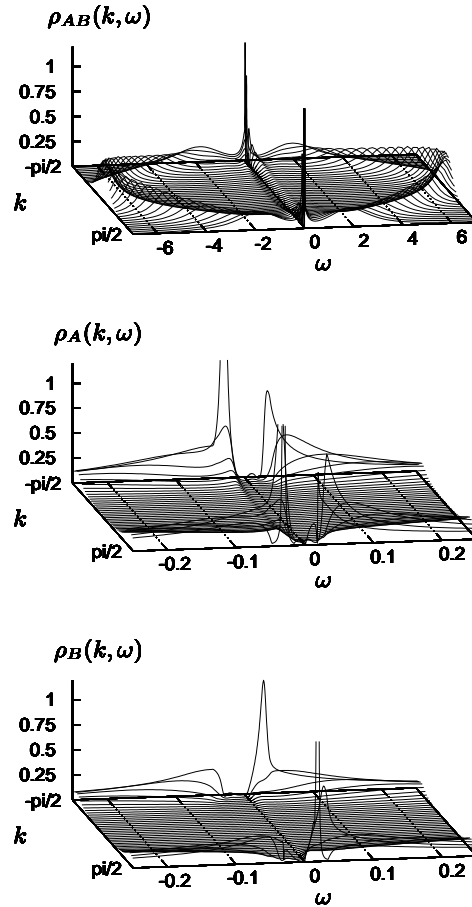


**Fig. 6.** [111]  $k$  resolved DMFT+NRG spectra with the same parameters as in Fig. 5. The top picture shows the whole spectrum for the combined DOS while the other two pictures show the partial DOS for the A and B sublattice for the region around the quasiparticle bands at the fermi level.

larly. This is demonstrated in Fig. 6, where the upper part gives an overall view of the total weight  $\rho_{AB}(\mathbf{k}, \omega)$  and the two lower parts magnify the region very near to the Fermi level  $\omega = 0$ .

Regarding the regions at large excitation energies  $\omega$  in the upper figure, considerable broadening and spreading of the resonances is observed compared to those of the Free Theory, see e.g. Fig. 3. Moreover, band splitting

due to the ionic field  $\Delta = \varepsilon_B - \varepsilon_A$  is not visible anymore and it seems that parts of the broadened band structure even have disappeared. Although the NRG treatment loses much accuracy away from the Fermi level due to the logarithmic discretization of energies, we attribute these findings to the dominance of scattering processes in this region due to the blocking effect on the effective sites. For the ionic version of the Hubbard model this seems to be of particular importance. Without the ionic field  $\Delta$  one may define the positions  $\omega_{\mathbf{k}}$  of broadened bands as usual [12] via the disappearance of the real part in the denominator of one particle Greens functions, i.e. solving for  $\Re \tilde{G}(\omega_{\mathbf{k}} + i\delta)^{-1} - \varepsilon_{\mathbf{k}} \equiv \omega_{\mathbf{k}} - \left( \varepsilon_{\mathbf{k}} + \frac{U}{2} + \Re \tilde{\Sigma}(\omega_{\mathbf{k}}) \right) = 0$  in the Hubbard model, where we have separated a Hartree-part  $\frac{U}{2}$  from the selfenergy of the effective Greens function  $\tilde{G}(z)$  and explicitly used its  $\mathbf{k}$ -independence in the effective site picture. Although  $\Re \tilde{\Sigma}(\omega + i\delta)$  bears a strong  $\omega$ -dependence, generally three solutions appear for the Hubbard model in the Fermi liquid regime which represent the two original  $U$ -split bands and the low-lying quasi-particle band. Level broadening occurs separately via  $\text{Im} \tilde{\Sigma}(\omega_{\mathbf{k}} + i\delta)$ . For the ionic Hubbard model the denominator of the Greens functions [10] mixes contributions of the two kinds of effective sites in a way that stresses the importance of scattering even more, i.e. one has to solve

$$\left( \omega_{\mathbf{k}} - \varepsilon_A - \Re \tilde{\Sigma}_A(\omega_{\mathbf{k}}) \right) \left( \omega_{\mathbf{k}} - \varepsilon_B - \frac{U}{2} - \Re \tilde{\Sigma}_B(\omega_{\mathbf{k}}) \right) - \text{Im} \tilde{\Sigma}_A(\omega_{\mathbf{k}} + i\delta) \cdot \text{Im} \tilde{\Sigma}_B(\omega_{\mathbf{k}} + i\delta) - \varepsilon_{\mathbf{k}}^2 = 0. \quad (13)$$

Roughly speaking,  $\text{Im} \tilde{\Sigma}_A(\omega_{\mathbf{k}} + i\delta) \approx \text{Im} \tilde{\Sigma}_B(\omega_{\mathbf{k}} + i\delta) \approx \Delta \varepsilon$  is a large energy shift for  $\omega_{\mathbf{k}}$  of order  $\varepsilon_A, \varepsilon_A + U$ , so that only the solutions, which are maximally removed from the Fermi level tend to remain in the high energy region after inclusion of the imaginary part of the self energies. In the low energy region, on the other hand, this effect is smallest near the Fermi level, which around half-filling makes the zone boundaries favourable for the existence of well defined quasi-particle bands. Thus we observe more pronounced resonances there as shown in the two lower parts of Fig. 6.

Apparently, the dominant parts of the quasi-particle bands reproduce the distribution of main spectral weight on the respective sublattice. The parts on the opposite side of the Fermi level, on the other hand, are shaped by admixtures, e.g. the spectral weight at the zone boundaries does not vanish anymore. Near the position of the ionic energies the NRG treatment combined with the effects described before leads to a less detailed band structure. This region is presumably described in a somewhat better way by the NCA calculation, see e.g. Fig. 7. Thus, our expectations that fundamental hybridization mechanisms, contained in the model, bear a relevance on the low lying states with many-body character, is supported. We have compiled SNCA and NRG results in our last Fig. 7 in order to provide an overall picture of the local DOS and both of its sublattice contributions. This also serves to underline our remarks about the usefulness of both calculational schemes in conjunction.

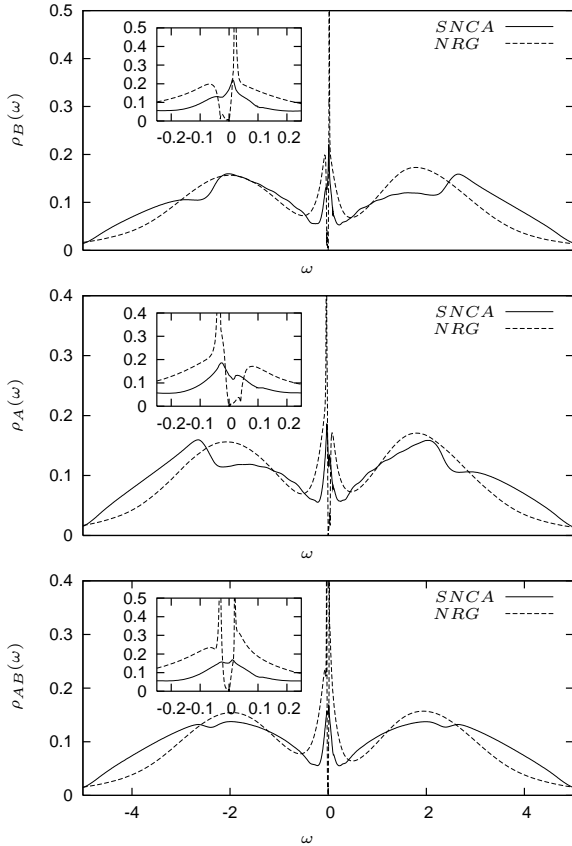


**Fig. 7.** Comparisons DOS obtained from DMFT with NRG and NCA for a  $3d$  simple cubic lattice. The insets show the region around the Fermi level in greater detail. The parameters used are the same as in Fig. 5; for the NCA a finite temperature  $1/T = \beta = 20$  was used. The NCA resolves much better the high energy features of the spectra but is not able to clearly resolve the quasiparticle hybridization gap as the NRG.

## 4 Conclusion

We have calculated correlated band structures of the ionic Hubbard model for a region of intermediate local repulsion at and near half-filling. The quasi-particle bands of low lying one-particle excitations show clear signatures of the underlying transfer (“hybridization”) mechanism contained in the noninteracting part of the Hamiltonian, in

particular with respect to a charge excitation gap and the distribution of spectral weight. We have motivated and interpreted these findings with reference to the Luttinger sum rule and to the dominantly local nature of the self-energy. Applying successively better approximations we tried to elucidate the transformation from a local ionic picture to essentially itinerant quasi-particle degrees of freedom and the correspondance to an intermediate tight binding scenario.

Using the SNCA in the DMFT selfconsisting cycle gave a good overall impression of the band structure and allowed for some qualitative conclusions about the low lying excitations. A satisfactory picture of the low energy region at low temperatures was nevertheless only achieved by application of the numerical renormalization group. Whether a full or improved NCA would allow for a more analytical approach and would lead to sensible results in this region, too, is still to be demonstrated. Altogether, the scope of controlling and understanding such calculations for complicated systems with more ionic species and realistic p- or d-shells, in the local approach or e.g. in the LDA-DMFT scheme [11], has been widened and improved: Some features of heavy quasi-particles seem definitely closely connected to a noninteracting system. Since the whole field at present rapidly develops to a stage, which is technically very much involved, this insight should be useful for future calculations.

As far as the existence of additional long ranged correlations and corresponding order parameters are concerned, a possible instability of the Fermi-liquid state considered

here towards magnetic order or towards phase separation should be investigated. Like in the homogeneous Hubbard model [31] knowledge of the one particle excitations is an important prerequisite for this program. Without further calculations our results demonstrate an asymmetry of occupation numbers  $n_A - n_B \neq 0$  away from half-filling [2], as a consequence of the asymmetric distribution of spectral densities, see e.g. Fig. 4(a, b).

## References

1. J. Hubbard and J. B. Torrance: Phys. Rev. Lett. **47**, 1750 (1981)
2. K. Pozgajcic and C. Gros: Phys. Rev. B **68**, 085106 (2003)
3. T. Wilkens and R. Martin: Phys. Rev. B **63**, 235108 (2001)
4. S. R. Manmana, V. Meden, R. M. Noack and K. Schönhammer: arXiv: cond-mat/0307741v1 (2003)
5. R. Zitzler, Th. Pruschke and R. Bulla: Euro. Phys. J. B **27**, 473 (2003)
6. N. Grewe and F. Steglich: Handbook Phys. and Chem. Rare Earths, Eds. K. A. Gschneidner jr. and L. Eyring, Elsevier, Amsterdam **14**, 343 (1991)
7. J. Sticht, N. D'Ambrumenil and J. Kübler: Z. Phys. B **65**, 149 (1986)
8. Th. Pruschke, M. Jarrell and J. K. Freericks, Adv. in Phys **42**, 187 (1995)
9. A. Georges, G. Kotliar, W. Krauth and M. J. Rozenberg: Rev. Mod. Phys. **68**, 13 (1996)
10. U. Brandt and Chr. Mielsch, Z. Phys. B **75**, 365 (1989)
11. K. Held, I. A. Nekrasov, N. Blümer, V. I. Anisimov and D. Vollhardt: Int. J. Mod. Phys. B **15**, 2611 (2001); M. B. Zöfl, Th. Pruschke, J. Keller, A. I. Poteryaev, I. A. Nekrasov and V. I. Anisimov: Phys. Rev. B **61**, 12810 (2000)
12. J. M. Luttinger: Phys. Rev. **119**, 1153 (1960)
13. R. M. Martin and J. W. Allen: J. Appl. Phys. **50**, 7561 (1979); R. M. Martin: Phys. Rev. Lett. **48**, 362 (1982)
14. N. Grewe: Z. Physik B - Cond. Matter **67**, 323 (1987)
15. N. Grewe: Solid State Commun. **50**, 19 (1984)
16. P. Fulde, J. Keller and G. Zwicknagl: Solid State Phys., Eds. H. Ehrenreich and D. Turnbull, Academic Press, San Diego **41**, 1 (1988)
17. Y. Kuramoto: Theory of Heavy Fermions and Valence Fluctuations, Eds. T. Kasuya and T. Saso, Springer, Berlin, 152 (1985); Ch. Kim, Y. Kuramoto and T. Kasuya: J. Phys. Soc. Japan **59**, 2414 (1990)
18. W. Metzner and D. Vollhardt: Phys. Rev. Lett. **62**, 324 (1989); W. Metzner: Physica B **165** & **166**, 403 (1990); D. Vollhardt: Correlated Electron Systems, Ed. V. Emery, World Scientific, Singapore (1993)
19. Th. Pruschke, R. Bulla and M. Jarrell: Phys. Rev. B **61**, 12799 (2000); R. Bulla, T. A. Costi and D. Vollhardt: Phys. Rev. B **64**, 045103-1 (2001)
20. Th. Pruschke and N. Grewe: Z. Physik B - Cond. Matter **74**, 439 (1989)
21. H. Keiter and J. C. Kimball: Int. J. Magn. **1**, 233 (1971); N. Grewe and H. Keiter: Phys. Rev. B **24**, 4420 (1981)
22. W. Metzner: Phys. Rev. B **43**, 8549 (1991)
23. N. Grewe: Z. Physik B - Cond. Matter **53**, 271 (1983)

24. Y. Kuramoto and H. Kojima: *Z. Physik B - Cond. Matter* **57**, 95 (1984);  
E. Müller-Hartmann: *Z. Physik B - Cond. Matter* **57**, 281 (1984);  
Y. Kuramoto and E. Müller-Hartmann: *J. Magn. Mat.* **52**, 122 (1985)
25. F. B. Anders and N. Grewe: *Europhys. Lett.* **26**, 551 (1994)
26. J. Kroha, P. Wölfle and T. A. Costi: *Phys. Rev. Lett.* **79**, 261 (1997)
27. K. G. Wilson, *Rev. Mod. Phys.* **47**, 773 (1975).
28. H. R. Krishna-Murty, J. W. Wilkins, and K. G. Wilson, *Phys. Rev. B* **21**, 1044 (1980).
29. R. Bulla, Th. Pruschke and A. C. Hewson, *J. Phys.: Condens. Matter* **9**, 10463 (1997).
30. R. Bulla, A. C. Hewson, and T. Pruschke, *J. Phys.: Condens. Matter* **10**, 8365 (1998).
31. M. Jarrell and Th. Pruschke: *Z. Physik B - Cond. Matter* **90**, 187 (1993);  
Th. Pruschke and R. Zitzler: arXiv: cond-mat/0309192v1 (2003)

